Received: 1 July 2023 | *Revised:* 2 September 2023 | *Accepted:* 28 September 2023
DOI: 10.37917/ijeee.20.2.9 *Early View* | *December 2024*

Iraqi Journal for Electrical and Electronic Engineering
Original Article

Open Access
IJEEE University of Basrah College of Engineering

An Experimental Investigation on VSI-fed Induction Motor using Xilinx ZYNQ-7000 SoC Controller

Santosh Yadav Maddu*[1], Dr. Nitin Ramesh Bhasme[2]
[1]Department of Electrical Engineering, Government College of Engineering, Aurangabad, Maharashtra, India
[2]Department of Electrical Engineering, Government College of Engineering, Yavatmal, Maharashtra, India

Correspondance
*Santosh Yadav Maddu
Research Scholar, Department of Electrical Engineering, Government College of Engineering, Chhatrapati Sambhajinagar, Maharashtra, India - 431005
Email: princesantoshyadav@gmail.com

Abstract
In medium voltage and high-power drive applications, pulse width modulation (PWM) techniques are widely used to achieve effective speed control of AC motors. In real-time, an industrial drive system requires reduced hardware complexity and low computation time. The reliability of the AC drive can be improved with the FPGA (field programmable gate array) hardware equipped with digital controllers. To improve the performance of AC drives, a new FPGA-based Wavect real-time prototype controller (Xilinx ZYNQ-7000 SoC) is used to verify the effectiveness of the controller. These advanced controllers are capable of reducing computation time and enhancing the drive performance in real-time applications. The comparative performance analysis is carried out for the most commonly used voltage source inverter (VSI)-based PWM techniques such as sinusoidal pulse width modulation (SPWM) and space vector pulse width modulation (SVPWM) for three-phase, two-level inverters. The comparative study shows the SVPWM technique utilizes DC bus voltage more effectively and produces less harmonic distortion in terms of higher output voltage, flexible control of output frequency, and reduced harmonic distortion at output voltage for motor control applications. The simulation and hardware results are verified and validated by using MATLAB/Simulink software and FPGA-based Wavect real-time controller respectively.

Keywords
Field programmable gate array, Motor control, Pulse width modulation, Voltage source inverter.

I. Introduction

In the last decade, extensive research has been conducted on power electronics-based electrical drives due to their vast applications in the power industry [1]. Major factors such as high efficiency, high density, and better electromagnetic capability are involved in the development of motor controllers. Due to evaluation in industrial power electronics integrated technologies, manufacturing costs would be reduced while reducing the volume and the weight of the controller with the enhancement of power density [2]. Three-phase voltage source inverters are commonly used in switched-mode power converters which demand a fixed switching frequency PWM signal and a constant duty cycle for controlling the output voltage of the inverter [3]. Because of their outstanding output quality and efficiency across the whole control range, three-phase voltage-source inverters are commonly used in motor drive systems [4]. It contains a DC link with a capacitive filter which feeds to a three-phase full-bridge having an inductor to mitigate the harmonic content. This topology enables low cost in hardware and reduces the control algorithm complexities. However, in practice, its non-linearity causes higher winding stress, higher noise, and a low operating range are serious factors which are needed to be addressed in Sensorless AC motor applications [5]. Pulse-width modulation (PWM) is becoming the usual method for operating inverter switches to achieve the needed output voltage [6, 7]. PWM techniques

have attracted the attention of the research community in the field of AC motor control applications. The different PWM topologies are developed for high-power and medium-voltage motor drives [8]. The major factors such as power level, machine type, and the power semiconductor devices decide the economic design of the power converter in AC drive systems concerning performance and cost [9, 10]. Among different PWM methods, SPWM and SVPWM for a two-level VSI are popularized in motor applications. These PWM techniques are utilized in vector-controlled AC motor drives to forecast the inverter switching instants from the modulating signals at the control output. In the SPWM method, a high-frequency carrier wave is compared to the modulating reference wave, then the intersection points decide the inverter switching instants. As in the SVPWM, the net reference voltage space vector can be divided into the sectors and then calculated by the switching times [11]. The SVPWM technique is very popular in Sensor and Sensorless vector control applications due to its high output power for the high-speed operation of the motor. It achieves higher DC bus utilization, low distortion in current waveform, and extended speed range of AC motor. The SPWM method is restricted for low-speed applications due to its higher THD compared to the SVPWM method [12]. However, the hardware implementation of the PWM techniques is very complex with limited accuracy. To address the aforementioned problems, simple and low-cost FPGA-based real-time digital controllers are preferred in vector-controlled AC motor drives [13]. A powerful FPGA platform is preferred in the digital domain to obtain high-performance power electronics. Earlier traditional microcontrollers or digital signal processing (DSP) relied on C/C++ programming languages whereas FPGA depended upon hardware description language (HDL). During the design process, extensive verification is highly required to optimize the required hardware design [14]. Using FPGA, the computation load can be highly reduced along with reduced power transistor switching losses. Moreover, the microprocessor or DSP needs a higher computation time compared to FPGA applications in machine model techniques of AC drives [15]. The complex SVPWM algorithms implemented using FPGA prove better results due to their high computational speed and inherent capability. However, in practice, the importance of advanced power electronics materials like Silicon Carbide (SiC) and Gallium Nitride (GaN) is rapidly increasing for power density requirement applications with FPGA. It enables motor controller capabilities to achieve a higher control bandwidth [16]. In this work, an FPGA-based Wavect real-time controller has been adopted due to its simplicity in hardware implementation, accuracy, fast response, and low-cost controller. Also, the parameters of the IM are shown in Table I. The specifications of the Wavect real-time controller are shown in Table II.

TABLE I.
THREE-PHASE INDUCTION MOTOR

S.No.	Squirrel cage type		
	Parameter	Value	Units
1	Stator Resistance, Rs	0.81	Ω
2	Rotor Resistance, Rr	0.49	Ω
3	Stator Inductance, Ls	264	mH
4	Rotor Inductance, Lr	372	mH
5	Magnetizing Inductance, Lm	0.1177	mH

II. SYSTEM DESIGN

A. Two level VSI

Inverters are the power converters at convert DC supply voltage into AC voltage. The purpose of an inverter is to manipulate the amplitude and frequency of the sine wave. In general, Three-phase, two-level voltage source inverters are widely used in medium-voltage and high-power drive applications [17]. Each leg of the inverter is of having two switches and a total of six switches. If the output of a switch is connected to the upper input terminal $+Vdc/2$ is positive otherwise, it is negative (lower terminal$-Vdc/2$). The output, v_{ao} or, pole voltage thus oscillates between$(+Vdc/2\ to -Vdc/2)$; The Sinusoidal modulating signals can be written in terms of the peak magnitude M,

$$\langle v_{leg,a} \rangle = V_{dc} \cdot d_a = \frac{V_{dc}}{2} M \,\mathrm{Sin}(2\pi ft) + \frac{V_{dc}}{2} \tag{1}$$

$$\langle v_{\mathrm{leg},b} \rangle = V_{dc} \cdot d_b = \frac{V_{dc}}{2} M \,\mathrm{Sin}(2\pi ft - 2\pi/3) + \frac{V_{dc}}{2} \tag{2}$$

$$\langle v_{leg,c} \rangle = V_{dc} \cdot d_c = \frac{V_{dc}}{2} M \,\mathrm{Sin}(2\pi ft + 2\pi/3) + \frac{V_{dc}}{2} \tag{3}$$

The duty cycles are computed as follows:

$$d_i = \frac{m_i}{2} + \frac{1}{2} \text{ where } i = a,b,c \tag{4}$$

The fundamental leg voltages will be,

$$\langle v_{leg,a} \rangle = V_{dc} \cdot d_a = \frac{V_{dc}}{2} M \,\mathrm{Sin}(2\pi ft) + \frac{V_{dc}}{2} \tag{5}$$

$$\langle v_{leg,b} \rangle = V_{dc} \cdot d_b = \frac{V_{dc}}{2} M \,\mathrm{Sin}(2\pi ft - 2\pi/3) + \frac{V_{dc}}{2} \tag{6}$$

$$\langle v_{leg,c} \rangle = V_{dc} \cdot d_c = \frac{V_{dc}}{2} M \,\mathrm{Sin}(2\pi ft + 2\pi/3) + \frac{V_{dc}}{2} \tag{7}$$

The fundamental line-to-line voltages

$$\langle v_{ab}\rangle = \langle v_{\text{leg},a}\rangle - \langle v_{\text{leg},b}\rangle = \frac{\sqrt{3}V_{dc}}{2} M\cos(2\pi ft - \pi/3) \quad (8)$$

$$\langle v_{bc}\rangle = \langle v_{\text{leg},b}\rangle - \langle v_{\text{leg},c}\rangle = \frac{\sqrt{3}V_{dc}}{2} M\cos(2\pi ft - \pi) \quad (9)$$

$$\langle v_{ca}\rangle = \langle v_{\text{leg},c}\rangle - \langle v_{\text{leg},a}\rangle = \frac{\sqrt{3}V_{dc}}{2} M\cos(2\pi ft + \pi/3) \quad (10)$$

Hence, the fundamental phase voltages (i.e., line-to-neutral):

$$\langle v_a\rangle = \frac{V_{dc}}{2} M\sin(2\pi ft) \quad (11)$$

$$\langle v_b\rangle = \frac{V_{dc}}{2} M\sin(2\pi ft - 2\pi/3) \quad (12)$$

$$\langle v_c\rangle = \frac{V_{dc}}{2} M\sin(2\pi ft + 2\pi/3) \quad (13)$$

Using the equations of phase voltages, load or phase can be written as follows

$$I_{a,RMS} = I_{b,RMS} = I_{c,RMS} = \frac{\sqrt{2}}{4} \frac{M_i V_{dc}}{\sqrt{R^2 + (2\pi fL)^2}} \quad (14)$$

Where M_i refers modulation index, R and L represent resistance and Inductance respectively.

In a Six-Step/ Square Wave Inverter, the phase-to-neutral voltage and the line-to-line voltage (in terms of the Fourier Series) can be written as

$$v_{an}(t) = \frac{2}{\pi} V_{dc}\left[\sin wt + \frac{1}{5}\sin 5wt + \frac{1}{7}\sin 7wt + \ldots.\right] \quad (15)$$

$$v_{ab}(t) = \frac{2\sqrt{3}}{\pi} V_{dc}\left[\sin\left(wt - \frac{\pi}{6}\right) + \frac{1}{5}\sin 5\left(wt - \frac{\pi}{6}\right) + \ldots\right] \quad (16)$$

B. PWM techniques

In the following subsections, different PWM techniques have been discussed.

1) Sinusoidal PWM

In SPWM, the three-phase modulating sinusoidal signal is compared to a high-frequency carrier signal to generate gate pulses at a fundamental frequency (50 Hz) for the inverter switches. Assume that the reference sine wave (Rotor output desired waveform) is compared to the carrier signal (Ramp ranges from 0 to 1). If the reference signal is a higher amplitude than the carrier signal amplitude then the switch is in an ON state (1) and if the reference signal is less than the carrier signal then the switch is in an OFF state (0). The amplitude modulation index is defined as "The peak value ratio of the sinusoidal modulating signal to the carrier wave peak" i.e., $K_\text{a} = V_\text{m}/V_\text{c}$

There are two regions named linear region of modulation and Over modulation that SPWM can operate. For the Linear region of modulation $0 < K_\text{a} \leq 1$, the inverter output voltage (phase or line) increases linearly with the Amplitude modulation index, K_a. For the Over-modulation $K_\text{a} > 1$, the inverter output voltage (phase or line) increases non-linearly with the Amplitude Modulation index, K_a. To implement the SPWM technique for Motor control applications, a high carrier frequency signal (Generally 10 kHz to 20 kHz) is generated from a microcontroller which is compared to a reference modulating signal (Generated from a controller). To avoid the harmonics mixed up with the fundamental frequency, the frequency of the carrier or ramp is at least 10 times greater than the fundamental frequency [8, 18]. The phase to neutral voltage can be written as,

$$v_{an} = 0.5V_{dc}\sin(wt) \quad (17)$$

2) Space vector PWM

In a three-phase inverter, the switches can turn on and off in eight unique states. By joining the sides of the vectors and making them into a hexagon. The main objective is to find the maximum phase to neutral voltage and generate the different switching patterns in a different way than the SPWM technique. Strictly speaking, it will look Cube in a three-dimensional view, the same seems to be a hexagon in two- a dimensional view. It is impossible to produce a voltage vector that is beyond this hexagon as a modulation would exceed a hundred percent which cannot happen. For Sine Wave generation, a voltage vector of constant magnitude is needed in every direction. The magnitude of the voltage vector is equal to the phase to neutral voltage. This voltage vector is obtained using the Clarke transform. The magnitude of the voltage vector doesn't change in the case of Clarke Transformation. By using Space Vector Modulation, there is 15% more voltage can be produced as compared to the SPWM technique [4]. In conventional SVPWM, the basic idea is to attain the desired voltage vector by taking the average of different possible states. However, the switching states are moving from one

period to another and require toggling two switches. Since these switches are not ideal cause more switching losses during on and off and vice versa. To overcome the transition problem, keeping the null vector in the middle position and simultaneously switching periods should be arranged. Since the sequence of applied voltages doesn't matter unless the timings are kept the same. In this, the net reference vector is rotating from one sector to another. This causes a double transition problem. To rectify it, the switching states would be swapped which is termed an alternate reverse sequence. This method of implementation is complex and switching losses are also higher [18]. The SVPWM method can also be realized as below with reduced computation time in real-time digital implementation:

In the Min-Max method, the main objective is to enhance the magnitude of the inverter output voltage by simply adding an offset to the reference signal. The resultant modulating signals can be written as [19],

$$\langle v_{am} \rangle = V_m \sin(wt) + offset \tag{18}$$

$$\langle v_{bm} \rangle = V_m \sin(wt - 2\pi/3) + offset \tag{19}$$

$$\langle v_{cm} \rangle = V_m \sin(wt + 2\pi/3) + offset \tag{20}$$

$$Here,\ Offset = -\frac{V_{\max} + V_{\min}}{2};$$

$$\mathrm{V}_{\max} = \mathrm{Max}\{v_{am}, v_{bm}, v_{cm}\}, \mathrm{V}_{\min} = \mathrm{Min}\{v_{am}, v_{bm}, v_{cm}\} \tag{21}$$

In Direct Injection of third harmonic PWM (THPWM), phase waveforms with no third harmonics can be created by adding third harmonics to the sinusoidal reference waveform. The modulating waves can be written as follows [8, 18],

$$\langle v_{am} \rangle = V_{m1} \sin(wt) + V_{m3} \sin(3wt) \tag{22}$$

$$\langle v_{bm} \rangle = V_{m1} \sin(wt - 2\pi/3) + V_{m3} \sin(3wt) \tag{23}$$

$$\langle v_{cm} \rangle = V_{m1} \sin(wt + 2\pi/3) + V_{m3} \sin(3wt) \tag{24}$$

The obtained modulation index can be written as,

$$|v_{am}| = \left| V_{m1} \sin(wt) - \frac{1}{3} V_{m1} \cos\left(\frac{\pi}{3}\right) \sin(3wt) \right| = 0.5 V_{dc} \tag{25}$$

C. Hardware implementation

In this work, The MATLAB/Simulink software results are validated and verified using an FPGA-based Wavect controller. The schematic hardware implementation of various PWM techniques for a two-level inverter is shown in Fig. 1

The most popular category of FPGA controllers is highly required for accurate response and position estimation [20]. Here, Fig. 2 represents the real-time experimental setup and, Fig. 3, shows the block diagram for a three-phase, two-level PWM inverter. The SVPWM switching states are represented as shown in Fig. 4. The experimental system consists of a Three-phase bridge rectifier, Autotransformer, Semikron inverter, Induction motor with load, and Wavect controller. DC capacitor bank serves to maintain the constant DC voltage at the inverter input side. The PWM signals and ADC interface is made through the Wavect Control board. The control algorithm can be implemented using HDL block sets of MATLAB/Simulink. After the implementation, the control algorithm is converted into HDL code generation using the HDL workflow advisor. The hardware implementation workflow and PI controller using HDL blocks in the WAVECT design suite are shown in Fig. 5 and Fig. 6 respectively. In this work, a V/f control algorithm is used to control the IM and its implementation is as shown in Fig. 7.

III. Result Analysis

For high-frequency applications, advanced control techniques (Field oriented control (FOC) and Direct torque control (DTC)) are often used PWM techniques in motor control drives. In General, a Six-step (Square) inverter produces more losses at the output of the inverter side.

The PWM techniques are more popular for AC drives due to their power loss in the switching devices being very low in the case of high-frequency applications. In this work, SPWM, Square Wave, SVPWM (Min-Max), and THPWM methods are implemented with the help of MATLAB/Simulink software. The results obtained in Simulink have shown phase voltage, line voltage, and load current without filter in Fig. 7, Fig. 8, Fig. 9, Fig. 10, and Fig. 11. Also, the FFT tool is used to analyze the performance of the motor by calculating the Total Harmonic Distortion (THD). The performance parameter, THD is calculated without filter for line and phase voltages of SPWM, Square wave type, THPWM, and SVPWM methods respectively. The Square wave type produces 61 % THD whereas other methods such as THPWM and SVPWM produce 53.47% THD approximately. From this, the SVPWM method produces less harmonic distortion compared to the SPWM method. The Comparative analysis is carried out for the PWM techniques at different switching frequencies. Table III and Table IV show %THD in-phase voltage and line voltage with fundamental phase and line voltages at 5 kHz

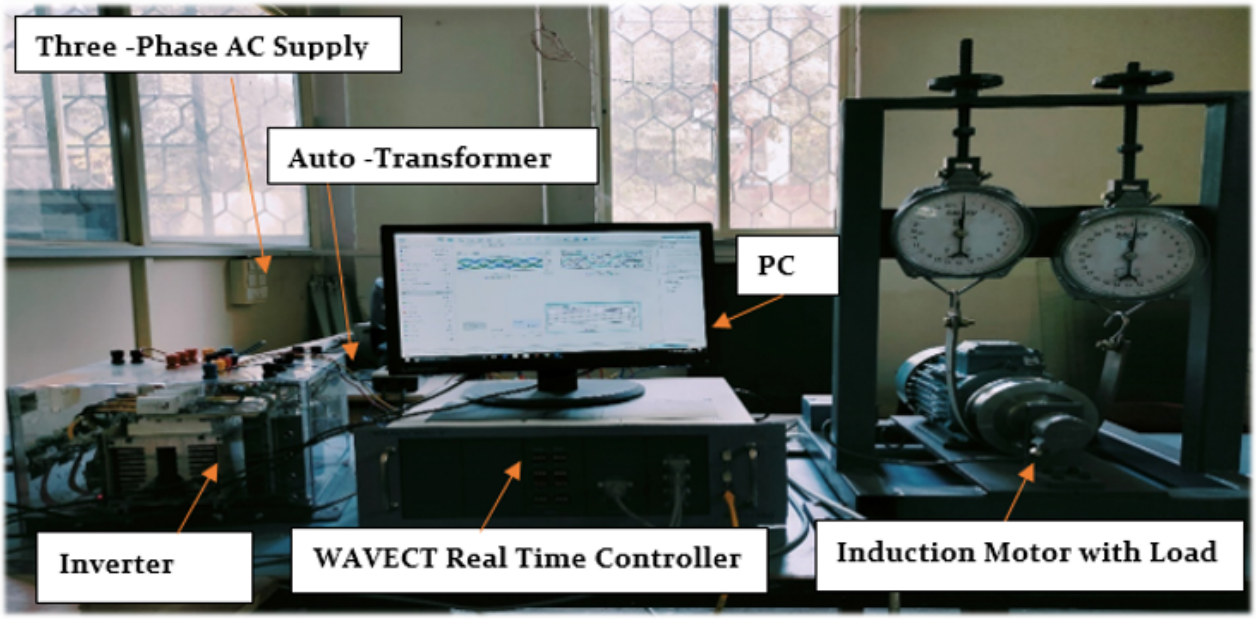

Fig. 1. Experimental lab setup of FPGA-based Wavect Controller

and 10 kHz respectively. The SVPWM technique using the Min-Max method has shown superior performance over other methods. In this paper, based on the Simulink results the most effective PWM methods for VSI-based two-level inverter is implemented using the Wavect Real-time controller. The control algorithm is implemented in MATLAB/Simulink and then converted into HDL code using HDL workflow. Wavect library enables the interfacing of MATLAB algorithm with the hardware and software. For SPWM, the reference sinusoidal voltage waves are compared with the carrier triangular wave, and load currents are observed in digital time control, similarly for SVPWM, reference voltages and the load current are obtained as shown in Fig. 12. Table V shows comparative hardware results of SPWM and SVPWM techniques with LC filter.

IV. Conclusion

There are numerous controllers are available in the literature to implement the PWM techniques. In this work, different pulse width modulation techniques have been studied and implemented by using a MATLAB/Simulink environment. The simulation results have shown that the SVPWM technique is better than the other conventional methods in terms of low total harmonic distortion (% THD) and better DC bus utilization. Then, a new FPGA-based Wavect controller is used to implement the conventional SPWM and SVPWM techniques. The control algorithm can be easily implemented by using FPGA-based Wavect real-time digital controllers and easily interfaces with MATLAB software. The most important conclusions have been drawn from the research work are as follows:

- To achieve high performance of AC drive, the SVPWM technique is suitable over other PWM methods for motor control algorithms.
- From Table V, SPWM has shown comparable results to SVPWM in terms of THD using an LC filter.
- The implementation of the SVPWM technique in the Min-Max method is quite easier compared to the other conventional techniques used in other standard controllers. Thus, the computation time is low in the absence of complex calculations or optimized algorithms.
- The controllers equipped with FPGA show quite fast responses with better accuracy. In this work, a new FPGA-based Wavect real-time prototype controller (Xilinx ZYNQ-7000 SoC) is introduced to verify the effectiveness of the controller for the existing PWM algorithms.
- Real-time digital controllers are useful for industrial control system applications to monitor the data continuously.
- Further, Wavect controller can be a better choice for the implementation of modern AC drives. This work can be extended to PWM-based motor control algorithms.

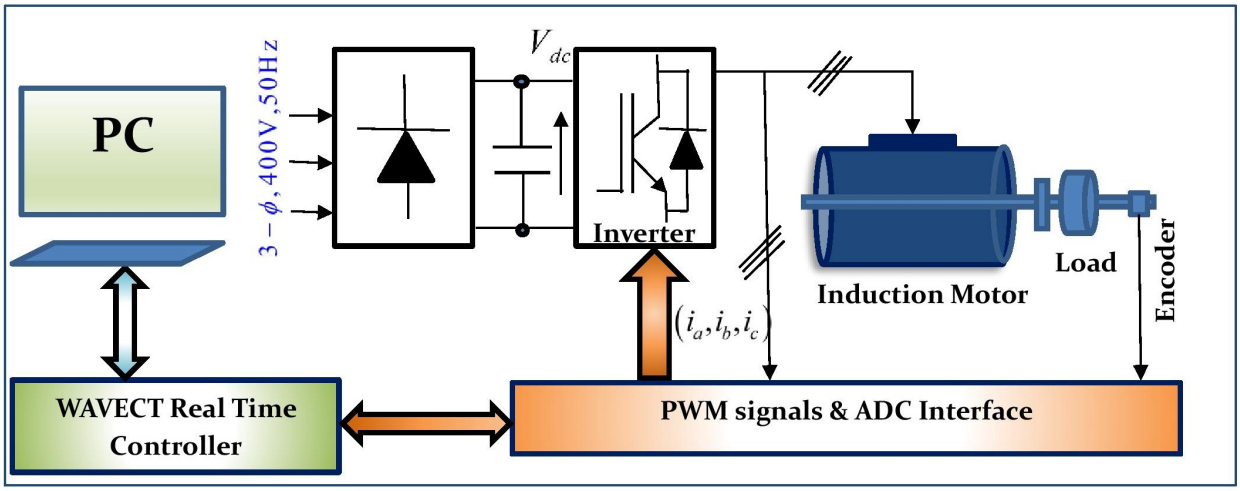

Fig. 2. Schematic of Wavect hardware setup

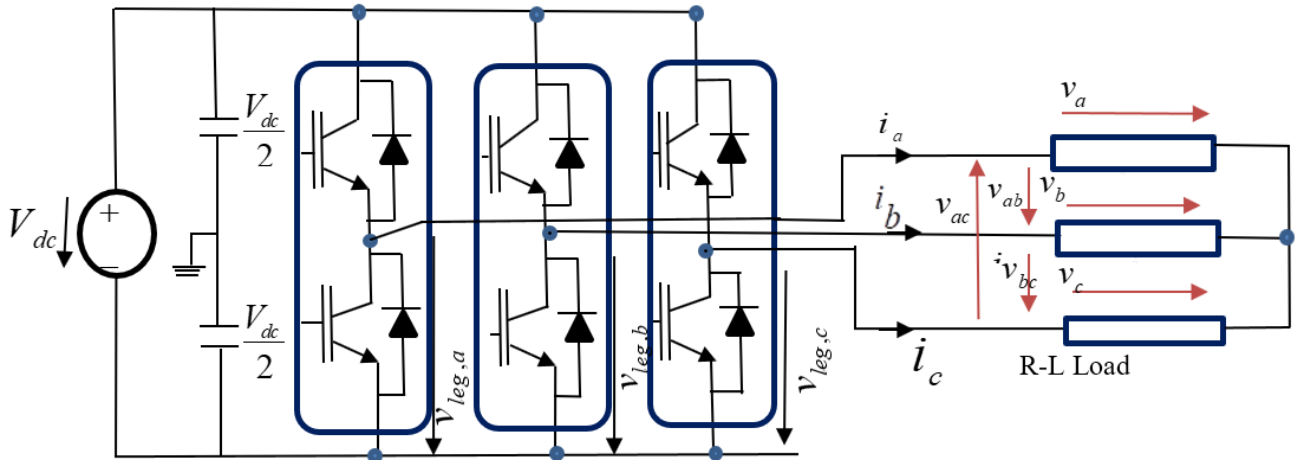

Fig. 3. Schematic of Three-phase, Two-level VSI with an RL load

ACKNOWLEDGMENT

The authors are thankful to AICTE, New Delhi for providing the National Doctoral Fellowship at the Department of Electrical Engineering, Government College of Engineering, Aurangabad, Maharashtra, India.

CONFLICT OF INTEREST

The authors have no conflict of relevant interest to this article.

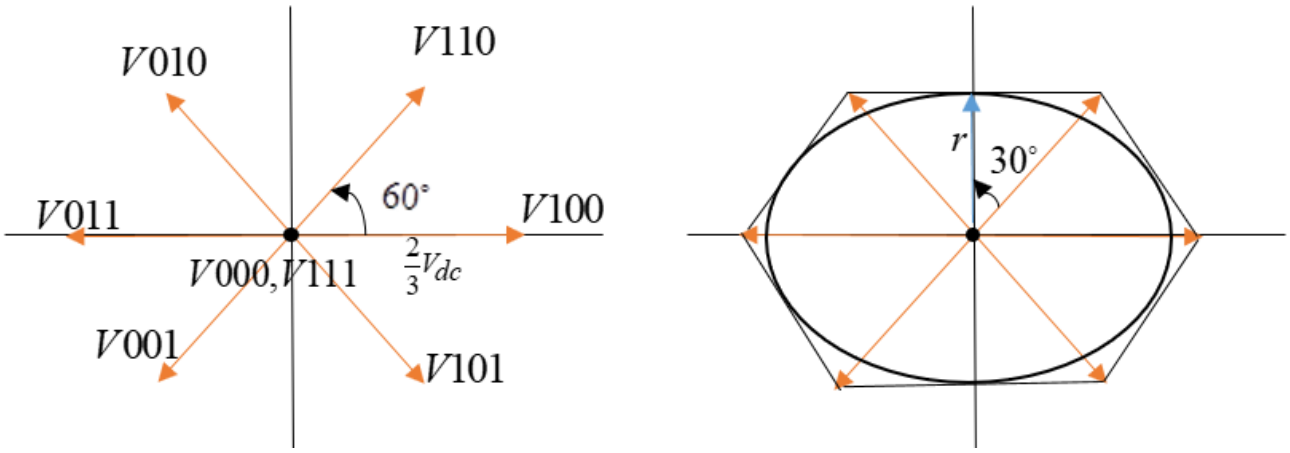

Fig. 4. Switching states and the maximum reference voltage vector in SVPWM

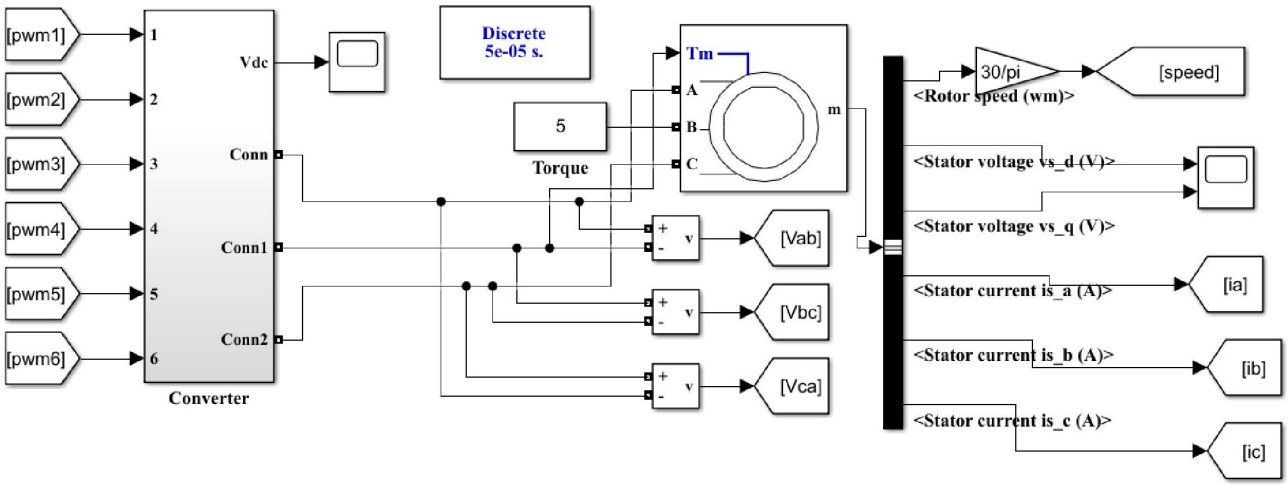

Fig. 5. Control algorithm implementation in WAVECT workflow

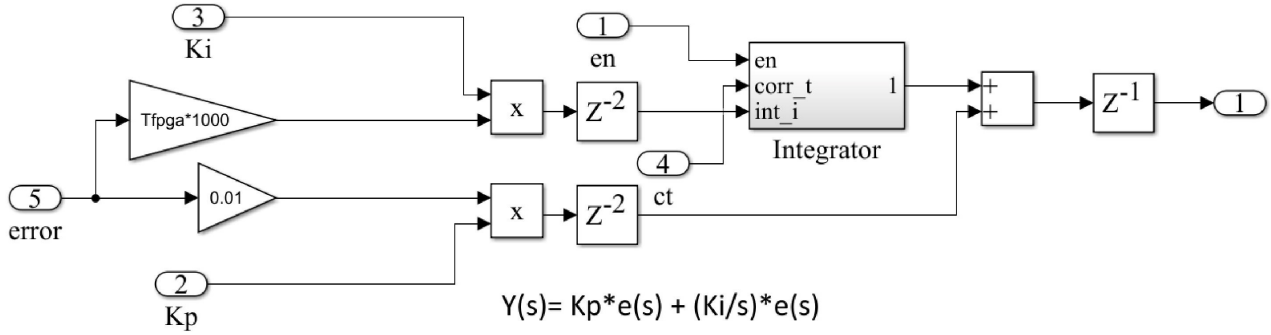

Fig. 6. PI controller implementation in the WAVECT design suite

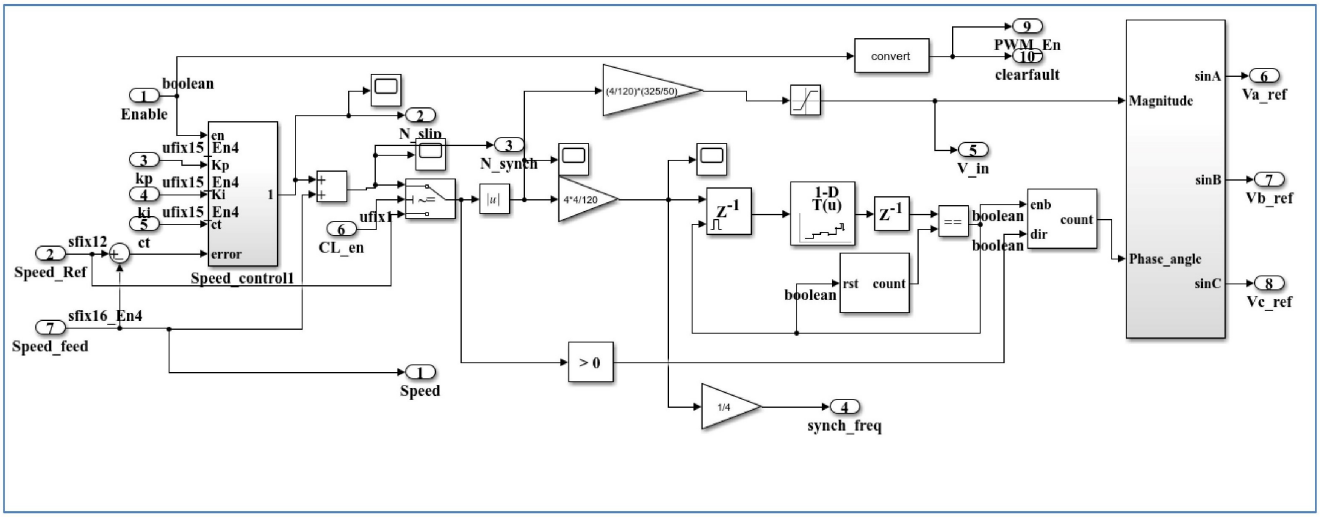

Fig. 7. Hardware HDL block implementation of VSI based on closed-loop control of Induction Motor

TABLE II.
WCU200 TECHNICAL SPECIFICATION

Parameter	**Specification details**
SoC	Xilinx ZYNQ-7000 SoC Dual ARM Cortex-A9 MPCore NEON Processing/FPU Engines Artix-7 Programmable FPGA
Memory	512 MB DDR3 256 Mb Quad-SPI Flash
Voltage Sensor	+/-1000V Measuring Range 4 to 16 Isolated Input Channels 16 Bit A/D Conversion
Current Sensor	25A RMS +/-85A Measuring Range Closed-loop Fluxgate Sensor 4 to 16 Isolated Inputs Channels 16 Bit A/D Conversion
PWM Output	12 to 60 Outputs 15V Voltage Level
Encoder Interface	Dual Encoder Interface
Relay Interface	4 NO/NC Outputs
Digital Inputs	4 Inputs(5V) with protection
Analog Outputs	+/-10V Output Range Eight Output Channels 16-Bit Resolution
Connectivity	1Gigabit Ethernet
Dimension	Approx. 480 x 400 x 175 mm

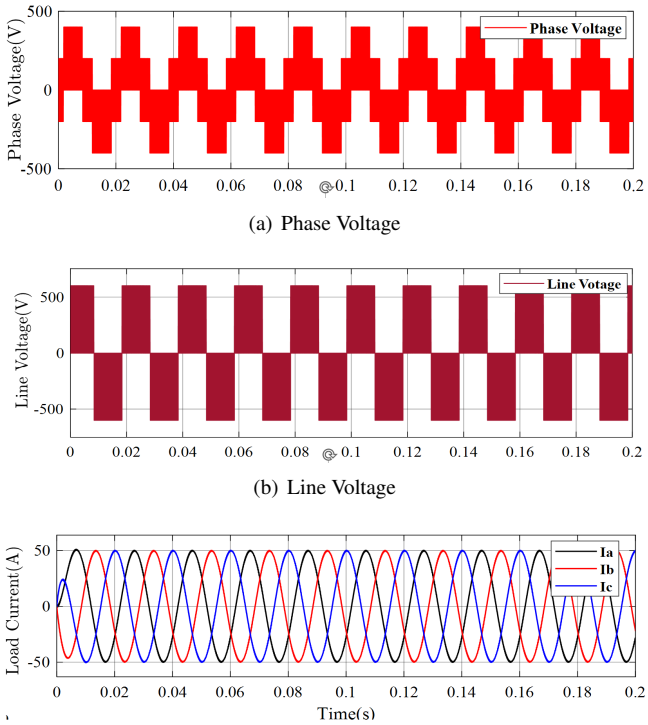

(a) Phase Voltage

(b) Line Voltage

(c) Load Current

Fig. 8. SPWM simulation results

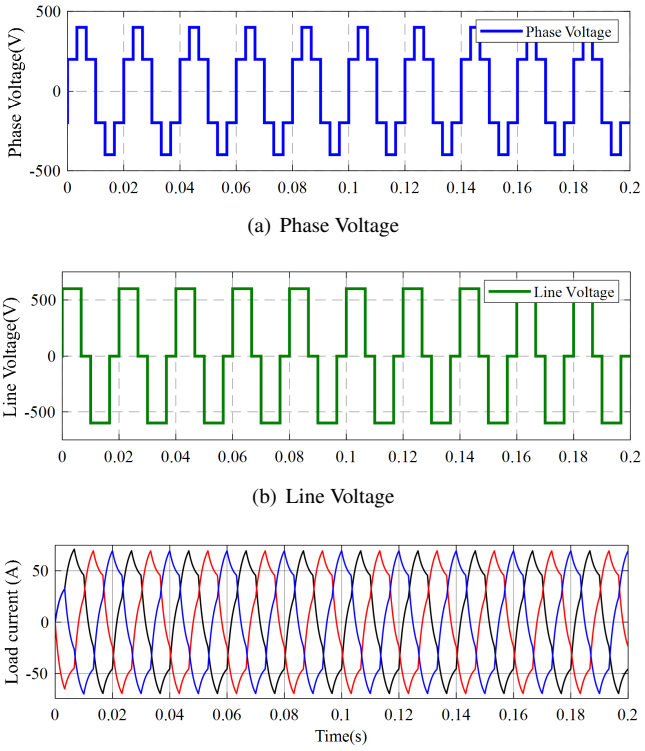

(a) Phase Voltage

(b) Line Voltage

(c) Load Current

Fig. 9. Square type simulation results

TABLE III.
COMPARATIVE SIMULATION ANALYSIS OF PWM TECHNIQUES AT 5 KHZ SWITCHING FREQUENCY

Parameter	**SPWM**	**THPWM**	**SVPWM (Min-Max)**
Phase Voltage(%THD)	70.53	53.47	53.59
Fundamental phase voltage (V)	294.2	342.3	343.1
Line Voltage(%THD)	70.60	53.58	53.44
Fundamental line voltage(V)	509.5	593	594.7

TABLE IV.
COMPARATIVE SIMULATION ANALYSIS OF PWM TECHNIQUES AT 10 KHZ SWITCHING FREQUENCY

Parameter	**SPWM**	**THPWM**	**SVPWM (Min-Max)**
Phase Voltage(%THD)	70.42	53.59	53.31
Fundamental phase voltage (V)	294.6	342.2	343.5
Line Voltage(%THD)	70.49	53.62	53.24
Fundamental line voltage(V)	510.1	593	595.2

TABLE V.
HARDWARE RESULTS FOR PHASE TO NEUTRAL VOLTAGES OF PWM TECHNIQUES

Phase to neutral	**SPWM**	**SVPWM (Min-Max)**
Phase Voltage(%THD), Van	5.11	5.19
Phase Voltage(%THD), Vbn	5.11	4.91
Phase Voltage(%THD), Vcn	5.04	4.94

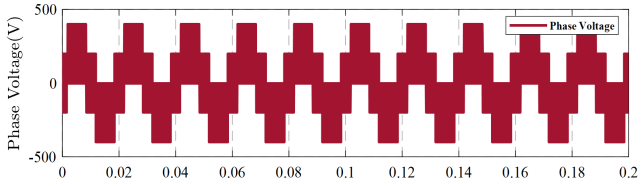

(a) Phase Voltage

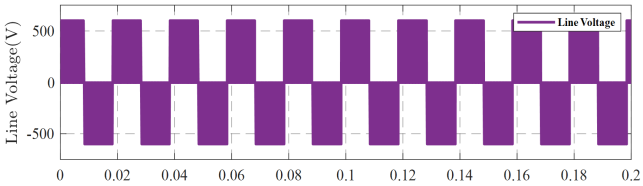

(b) Line Voltage

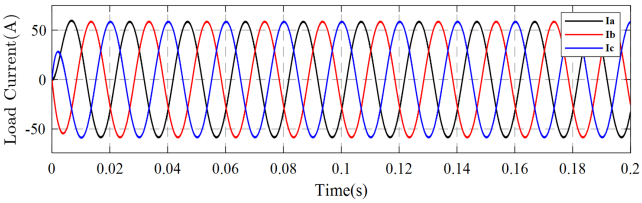

(c) Load Current

Fig. 10. SVPWM (Min-Max) simulation results

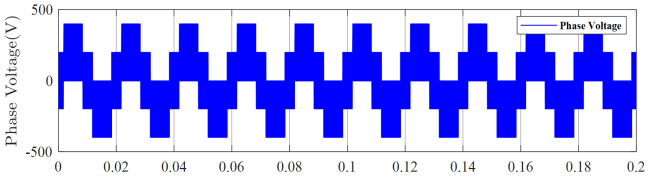

(a) Phase Voltage

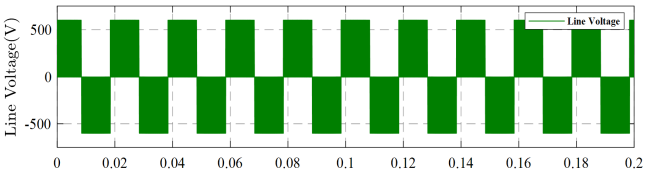

(b) Line Voltage

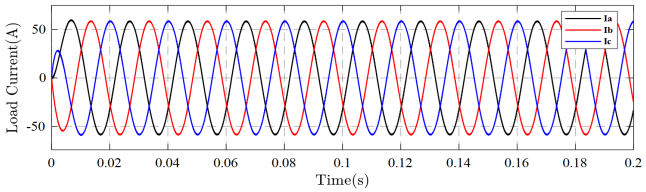

(c) Load Current

Fig. 11. THPWM simulation results

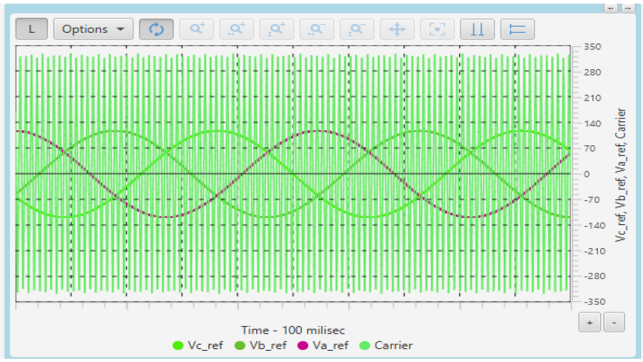

(a) Reference and Carrier Signal generation for SPWM

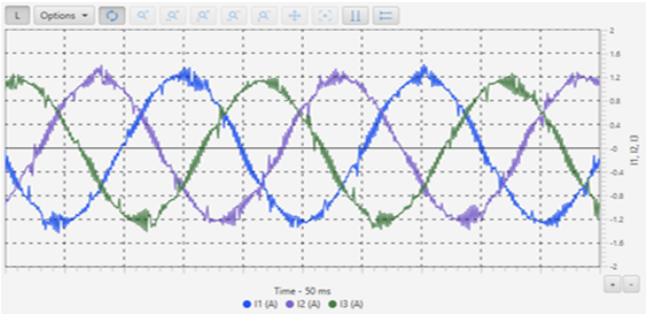

(b) Phase Currents in SPWM

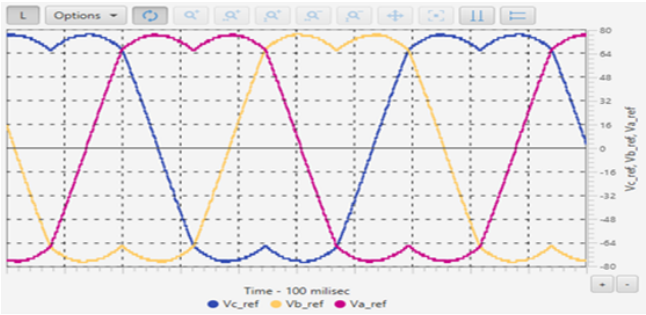

(c) Reference signal in SVPWM (Min-Max)

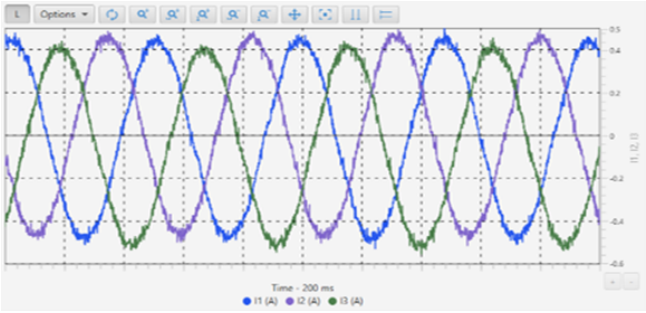

(d) Phase currents in SVPWM (Min-Max)

Fig. 12. Hardware results

REFERENCES

[1] X. Qi and J. Holtz, "Modeling and control of low switching frequency high-performance induction motor drives," *IEEE Transactions on Industrial Electronics*, vol. 67, no. 6, pp. 4402–4410, 2020.

[2] W. Cai, X. Wu, M. Zhou, Y. Liang, and Y. Wang, "Review and development of electric motor systems and electric powertrains for new energy vehicles," *Automotive Innovation*, vol. 4, pp. 3–22, 2021.

[3] S. B. Santra, K. Bhattacharya, T. R. Chudhury, and D. Chatterjee, "Generation of pwm schemes for power electronic converters," in *2018 20th National Power Systems Conference (NPSC)*, pp. 1–6, IEEE, 2018.

[4] P. Divyasree and A. Binojkumar, "Vector control of voltage source inverter fed induction motor drive using space vector pwm technique," in *2017 International Conference on Energy, Communication, Data Analytics and Soft Computing (ICECDS)*, pp. 2946–2951, IEEE, 2017.

[5] H. Mohan, M. K. Pathak, and S. K. Dwivedi, "Sensorless control of electric drives–a technological review," *IETE Technical Review*, vol. 37, no. 5, pp. 504–528, 2020.

[6] D. Holmes and G. Lipo, "A. thomas a."pulse width modulation for power converters–principle and practice," 2003.

[7] H. Chen and H. Zhao, "Review on pulse-width modulation strategies for common-mode voltage reduction in three-phase voltage-source inverters," *IET Power Electronics*, vol. 9, no. 14, pp. 2611–2620, 2016.

[8] S.-H. Kim, "Pulse width modulation inverters," *Electric Motor Control*, vol. 17, pp. 265–340, 2017.

[9] S. Dabour, M. Hussien, A. Aboushady, and M. E. Farrag, "Sensorless speed observer for industrial drives based induction motors with low complexity," in *Induction Motors-Recent Advances, New Perspectives and Applications*, IntechOpen, 2023.

[10] Z. Tir, T. Orlowska-Kowalska, H. Ahmed, and A. Houari, "Adaptive high gain observer based mras for sensorless induction motor drives," *IEEE Transactions on Industrial Electronics*, 2023.

[11] M.-F. Tsai, C.-S. Tseng, and P.-J. Cheng, "Implementation of an fpga-based current control and svpwm asic with asymmetric five-segment switching scheme for ac motor drives," *Energies*, vol. 14, no. 5, p. 1462, 2021.

[12] S. Y. Maddu and N. R. Bhasme, "Performance analysis of direct torque control of induction motor using snetly real-time controller," in *2022 19th International Conference on Electrical Engineering, Computing Science and Automatic Control (CCE)*, pp. 1–6, IEEE, 2022.

[13] S. Y. Maddu and N. R. Bhasme, "Performance investigation of vector control-based induction motor using snetly controller," *SSRG International Journal of Electrical and Electronics Engineering*, vol. 9, no. 12, pp. 109–119, 2022.

[14] J. S. Lee and G. Choi, "Modeling and hardware-in-the-loop system realization of electric machine drives—a review," *CES Transactions on Electrical Machines and Systems*, vol. 5, no. 3, pp. 194–201, 2021.

[15] S. Y. Maddu and N. R. Bhasme, "Performance analysis of ekf-based sensorless induction motor drive using fpga controller," in *2023 13th International Symposium on Advanced Topics in Electrical Engineering (ATEE)*, pp. 1–6, IEEE, 2023.

[16] J. Walden, H. K. Bai, B. Cheng, and F. Jin, "High frequency injection sensorless control for a permanent magnet synchronous machine driven by an fpga controlled sic inverter," in *2021 IEEE 8th Workshop on Wide Bandgap Power Devices and Applications (WiPDA)*, pp. 194–198, IEEE, 2021.

[17] Y. Huang, J. Walden, A. Foote, H. Bai, D. Lu, F. Jin, and B. Cheng, "Analytical characterization of cm and dm performance of three-phase voltage-source inverters under various pwm patterns," *IEEE Transactions on Power Electronics*, vol. 36, no. 4, pp. 4091–4104, 2020.

[18] H. Abu-Rub, A. Iqbal, and J. Guzinski, *High performance control of AC drives with Matlab/Simulink*. John Wiley & Sons, 2021.

[19] M. M. Gaballah, "Design and implementation of space vector pwm inverter based on a low cost microcontroller," *Arabian journal for science and engineering*, vol. 38, pp. 3059–3070, 2013.

[20] S. Yadav and N. Bhasme, "Performance analysis of sensorless induction motor drive using improved control techniques," *International Journal of Electrical and Electronics Research (IJEER)*, vol. 11, no. 4, pp. 1022–1029, 2023.